Molecular Cell, Volume *64*

Supplemental Information

Intercellular Coupling of the Cell Cycle and Circadian Clock in Adult Stem Cell Culture

Toru Matsu-ura, Andrey Dovzhenok, Eitaro Aihara, Jill Rood, Hung Le, Yan Ren, Andrew E. Rosselot, Tongli Zhang, Choogon Lee, Karl Obrietan, Marshall H. Montrose, Sookkyung Lim, Sean R. Moore, and Christian I. Hong

List of Supplemental Information

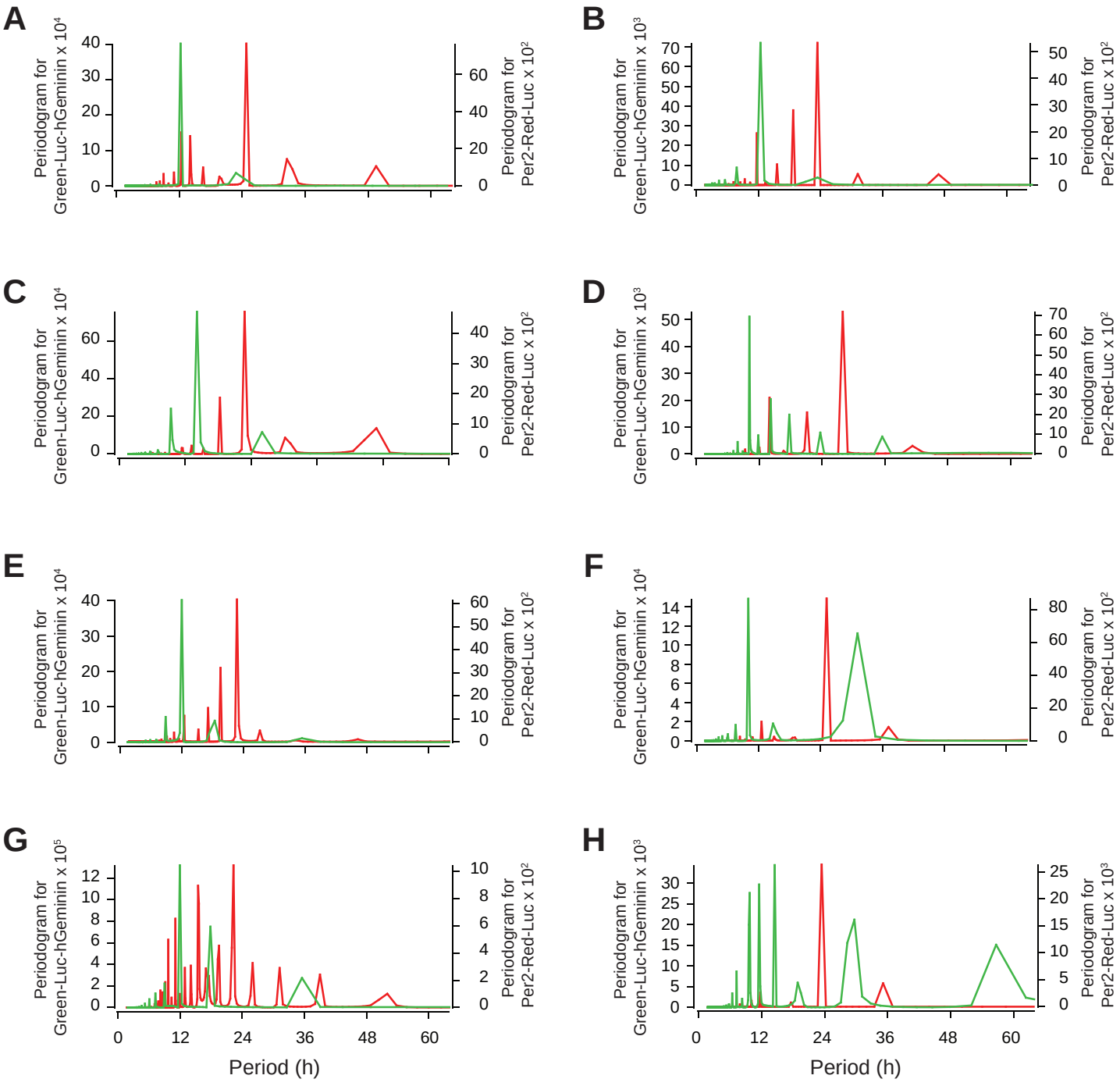
A
B
C
D
E
F
G
H
Periodogram for Green-Luc-hGeminin x 10^4
Periodogram for Per2-Red-Luc x 10^2
Period (h)
0
12
24
36
48
60

Figure S1

Figure S1 FFT analysis of Green-Luciferase-hGeminin and *Per2*-Red-Luciferase traces in the population of mouse enteroids, Related to Figure 1. (A-H) Spectra of FFT analysis of Green-Luciferase-hGeminin (green) and *Per2*-Red-Luciferase (red) traces in the population of mouse enteroids. The major peak of Green-Luciferase-hGeminin and *Per2*-Red-Luciferase was used to determine the frequency of the oscillations of cell cycle and circadian clock, respectively.

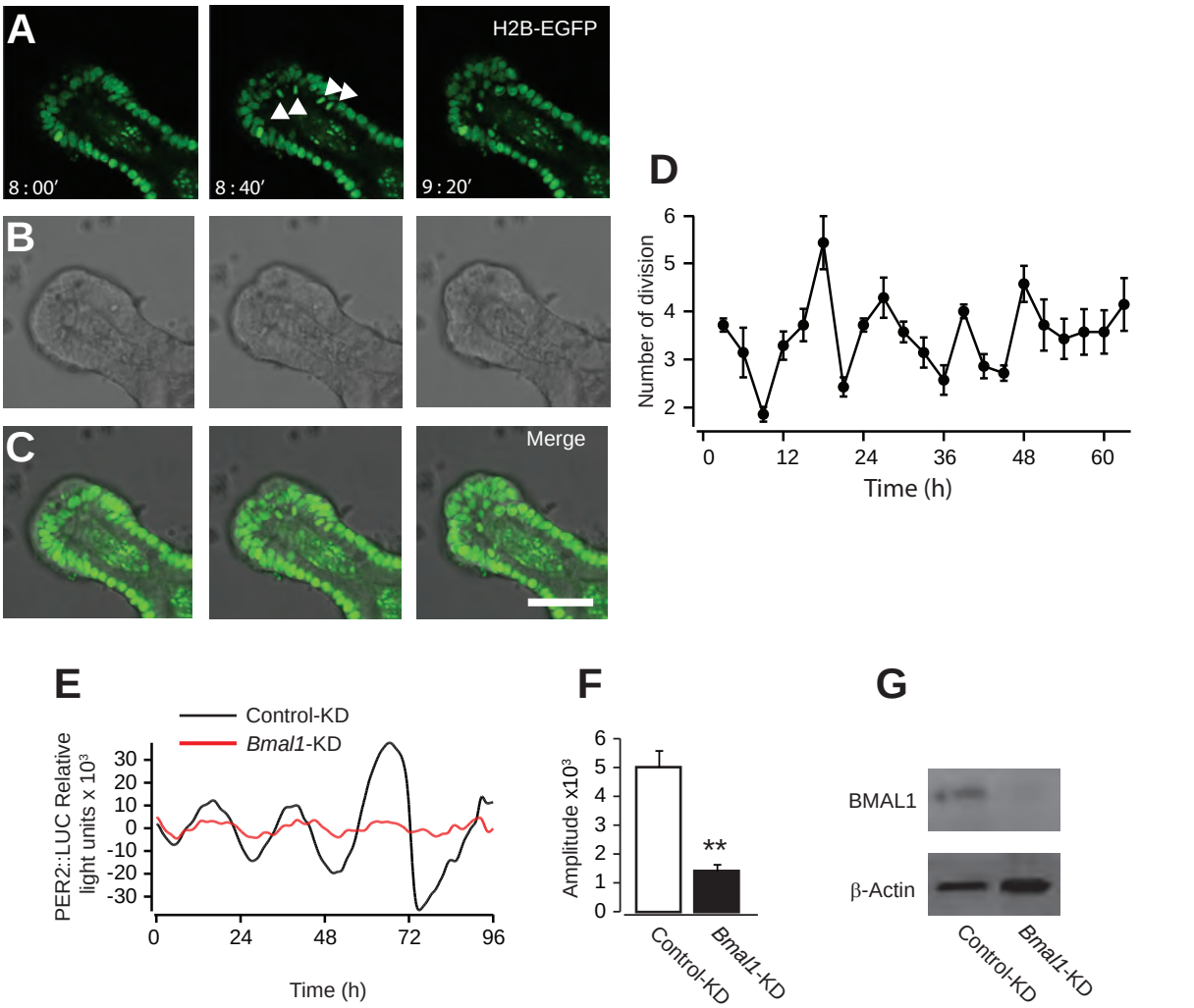
A
H2B-EGFP
8 : 00′
8 : 40′
9 : 20′
B
C
Merge
D
Number of division
Time (h)
E
Control-KD
Bmal1-KD
PER2::LUC Relative light units x 10³
Time (h)
F
Amplitude x10³
**
Control-KD
Bmal1-KD
G
BMAL1
β-Actin
Control-KD
Bmal1-KD

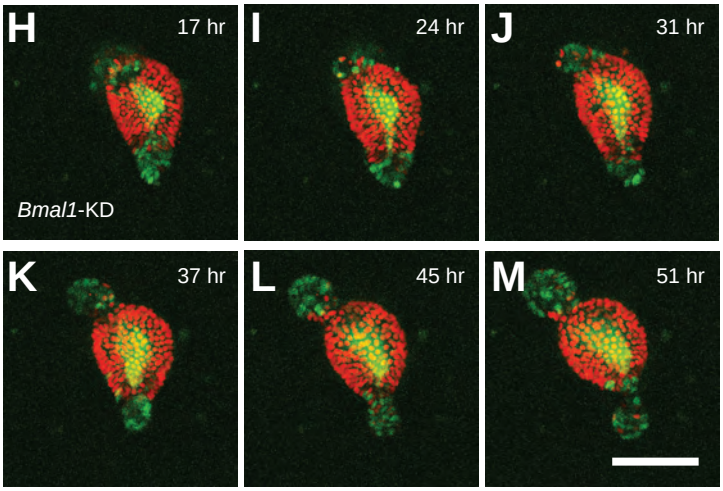
H
17 hr
Bmal1-KD
I
24 hr
J
31 hr
K
37 hr
L
45 hr
M
51 hr

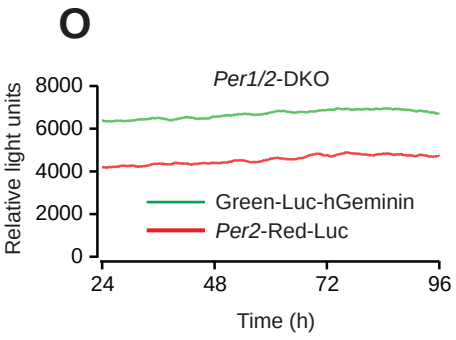
O
Per1/2-DKO
Relative light units
Green-Luc-hGeminin
Per2-Red-Luc
Time (h)

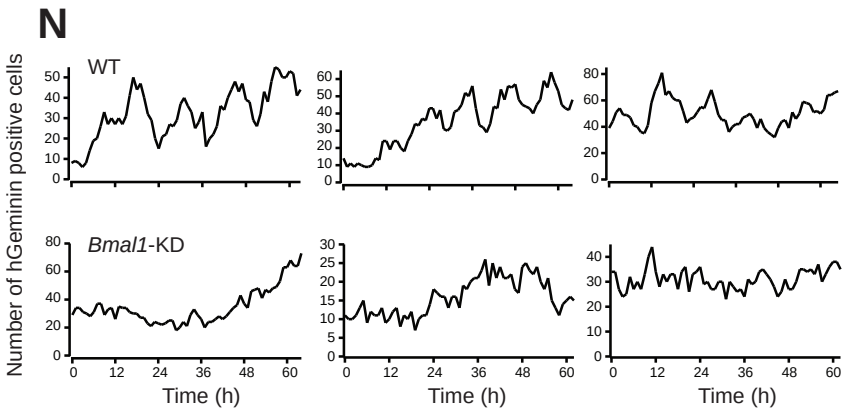
N
WT
Bmal1-KD
Number of hGeminin positive cells
Time (h)
Time (h)
Time (h)

Figure S2

Figure S2 Cell cycle progression in H2B-EGFP, *Bmal1*-KD, and control-KD enteroids, Related to Figure 2 (A-C) Fluorescent (A), phase contrast (B), and merged (C) images showing cell divisions of EGFP expressing cells in the enteroid derived from H2B-EGFP transgenic mice. Scale bar, 50 μm. Arrow heads indicate the dividing cells. (D) Number of divisions at crypt against the experimental time. n = 3. Single experiment contains 5-11 enteroids. Error bars correspond to the SEM. (E) Representative traces of PER2::LUC signal in control-KD (black line) and *Bmal1*-KD (red line) enteroids. (F) Average amplitudes of oscillations of PER2::LUC signal in control-KD (white bar, n = 6) and *Bmal1*-KD (n = 5) enteroids. Error bars correspond to the SEM. **: $p < 0.01$, student's test. (G) Expression levels of BMAL1 and β-ACTIN in control-KD and *Bmal1*-KD FUCCI enteroids were determined by western-blots. The KD efficiency of *Bmal1* was 84.2 ± 12.3% (mean ± SD). (H-M) Images showing spatial distribution of mVenus-hGeminin (green: S-G2-M) and mCherry-hCdt1 (red: G0/G1) in a *Bmal1*-KD FUCCI2 enteroid. Scale bar, 100 μm. (N) Representative raw traces of number of mVenus-hGeminin (green) and mCherry-hCdt1 (red) positive cells in a single WT (upper panels) or *Bmal1*-KD (lower panels) FUCCI2 enteroid. (O) Representative traces of signal changes of Green-Luciferase-hGeminin (green) and *Per2*-Red-Luciferase (red) in a population of *Per1/2*-DKO enteroids.

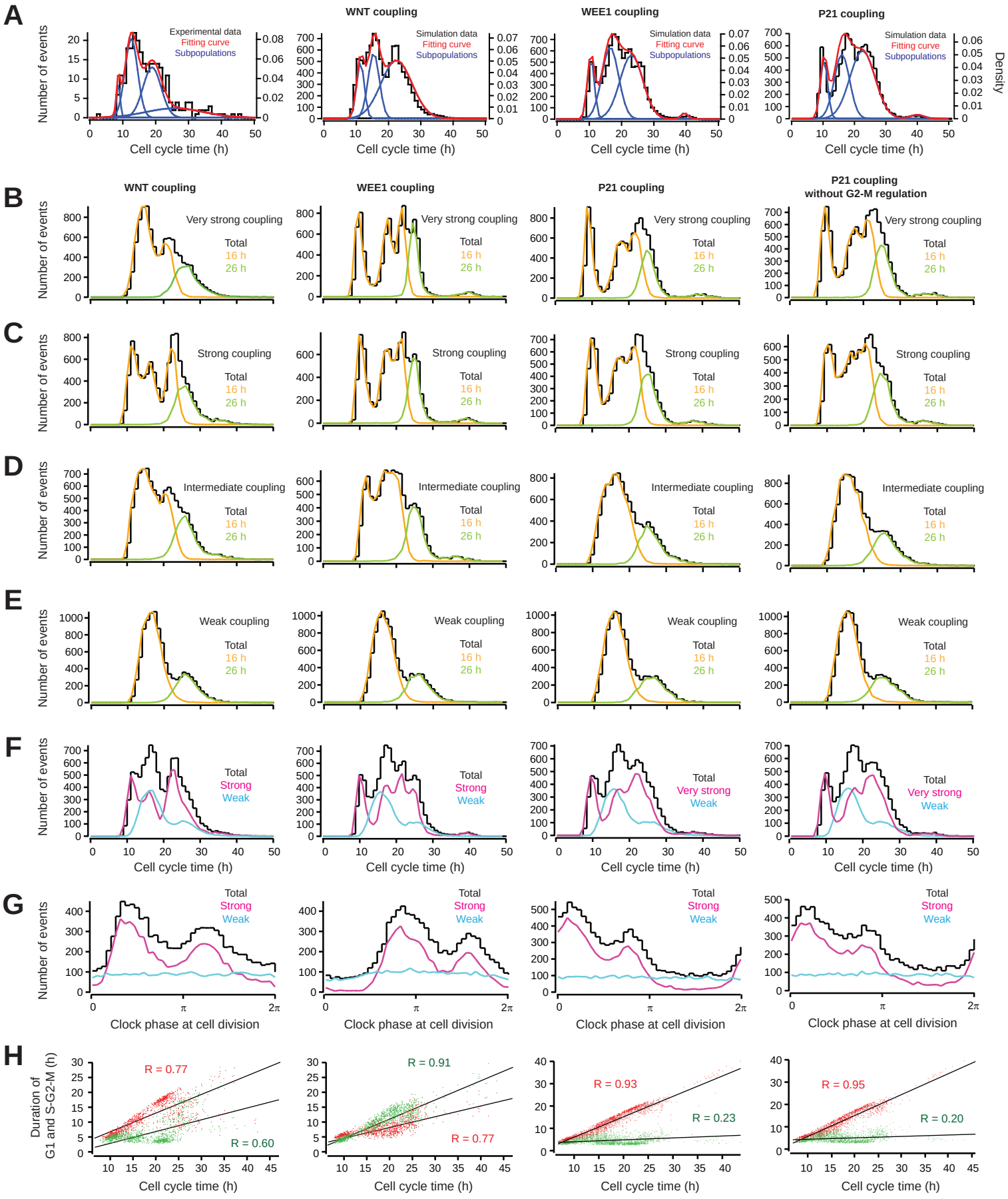
A
WNT coupling
WEE1 coupling
P21 coupling
Experimental data
Simulation data
Fitting curve
Subpopulations
Number of events
Density
Cell cycle time (h)
B
P21 coupling
without G2-M regulation
Very strong coupling
C
Strong coupling
D
Intermediate coupling
E
Weak coupling
Total
16 h
26 h
F
Strong
Weak
Very strong
G
Clock phase at cell division
H
Duration of
G1 and S-G2-M (h)
R = 0.77
R = 0.60
R = 0.91
R = 0.77
R = 0.93
R = 0.23
R = 0.95
R = 0.20

Figure S3

Figure S3 Stochastic simulations of the distribution of cell cycle time, Related to Figure 3
Experimental and simulated histograms with WNT, WEE1, and P21 coupling models. P21 is known to inhibit cell cycle progression at both G1/S and G2/M transitions, and its expression is known to be controlled by CLOCK/BMAL1 complex (Grechez-Cassiau et al., 2008). We considered the gating of P21 at only at G1/S or both G1/S and G2/M transitions. (A) Fitting curves (red and blue curves) for experimental and simulated histograms (black lines) of cell cycle times. Histograms from FUCCI2 enteroids, simulated histograms in the model with WNT, WEE1, and P21 coupling are shown from left to right, respectively. Gaussian mixture distribution revealed five peaks in FUCCI2 enteroids, WNT model, and WEE1 models (Experimental data: 8.7 ± 0.6 h, 12.6 ± 1.9 h, 18.9 ± 2.8 h, and 25.8 ± 8.7 h, WNT: 11.3 ± 1.2 h, 15.4 ± 1.7 h, and 22.4 ± 4.8 h, WEE1: 10.5 ± 1.1 h, 16.5 ± 2.6 h, 23.1 ± 3.5 h, and 39.5 ± 1.1 h, mean ± SD). Four peaks were found in p21 model. Blue curves are fitting curves for the subpopulations (P21: 10.3 ± 1.1 h, 16.0 ± 2.4 h, 22.5 ± 4.0, and 36.9 ± 2.2). Results from 10,000 cells are shown for simulated histograms. (B-E) Simulated histograms of distributions of cell cycle times in the model with WNT, WEE1, P21, and P21 without G2-M regulation coupling from left to right, respectively. Histograms simulated with very strong (B: 7,500 cells), strong (C: 7,500 cells), intermediate (D: 2,500 cells), and weak (E: 2500 cells) coupling strengths are shown. Population of cells with the average cell cycle time of 16 h (yellow lines), 26 h (green lines), and sum of 75% of 16 h and 25% of 26 h cells (histograms) are shown. (F) Histograms with sum of 65% of strong coupling (pink lines) and 35% of weak coupling (light blue lines) are shown for Wnt and Wee1 coupling models, respectively (10,000 cells). And histograms with sum of 65% of very strong coupling (pink lines) and 35% of weak coupling (light blue lines) are shown for P21 and P21 without G2-M regulation coupling models, respectively (10,000 cells). (G) Simulated histograms of timing of cell divisions relative to clock phase in WNT, WEE1, P21, and P21 without G2-M regulation coupling models from left to right, respectively (10,000 cells). (H) Relationship between CCT and duration of S-G2-M (green dots) or G1 (red dots) in WNT, WEE1, P21, P21 without G2-M regulation coupling models from left to right, respectively (n = 1,000). Black lines are the regression lines. Correlation coefficients are shown on the graph. The values of coupling parameters used in the simulations are: WNT coupling: (B) $k_{w4}' = 0$, $k_{w4} = 3$, (C) $k_{w4}' = 0$, $k_{w4} = 2$, (D) $k_{w4}' = 1$, $k_{w4} = 1$, (E) $k_{w4}' = 2$, $k_{w4} = 0.25$, WEE1 coupling: (B) $k_{w5}' = 0.25$, $k_{w5} = 3$, (C) $k_{w5}' = 0.25$, $k_{w5} = 2$, (D) $k_{w5}' = 0.5$, $k_{w5} = 1$, (E) $k_{w5}' = 1$, $k_{w5} = 0.25$, P21 coupling: (B) $k_{w3}' = 0$, $k_{w3} = 80$, (C) $k_{w3}' = 0$, $k_{w3} = 60$, (D) $k_{w3}' = 10$, $k_{w3} = 20$, (E) $k_{w3}' = 15$, $k_{w3} = 5$.

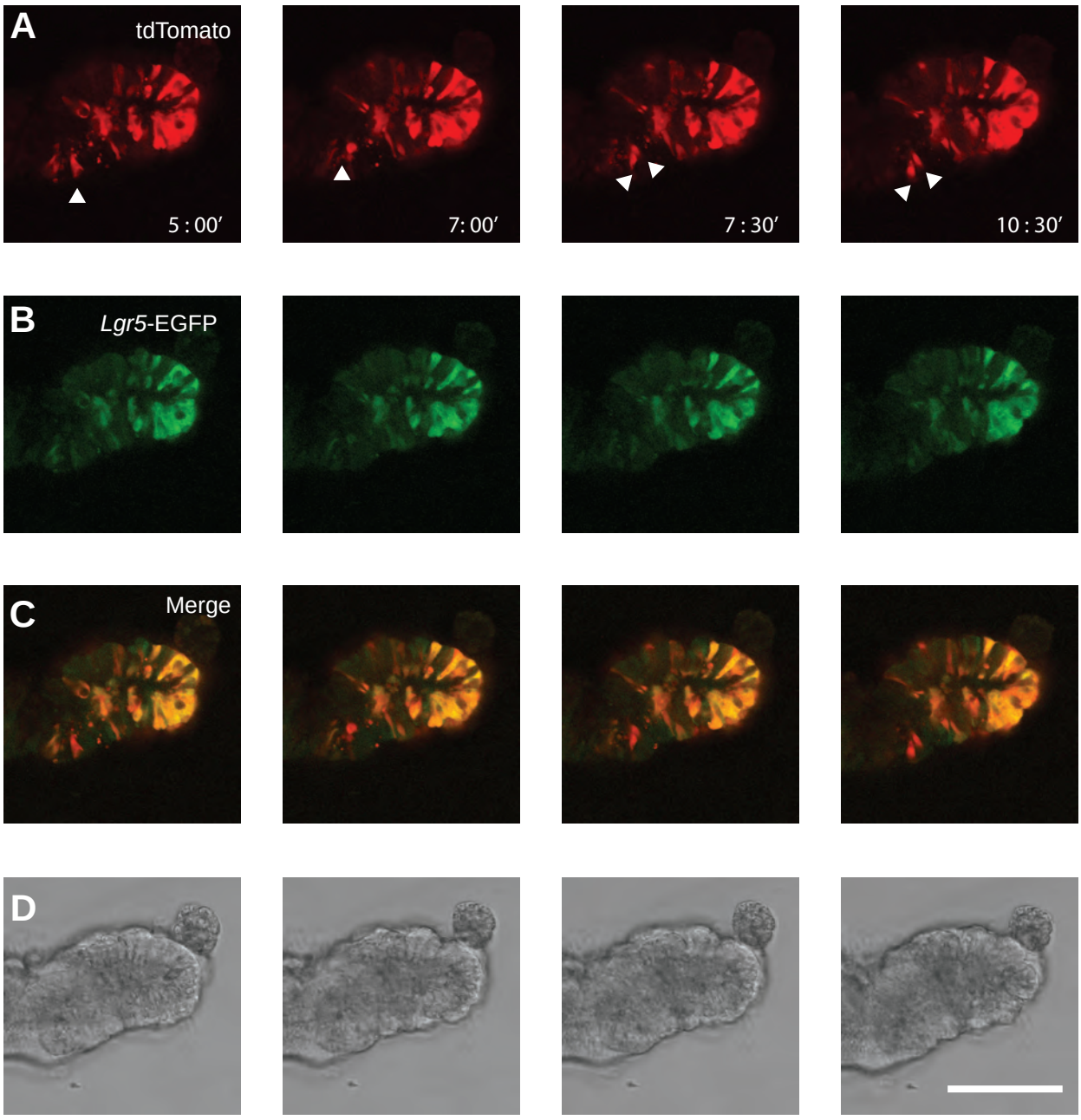
A
tdTomato
5 : 00′
7: 00′
7 : 30′
10 : 30′
B
Lgr5-EGFP
C
Merge
D

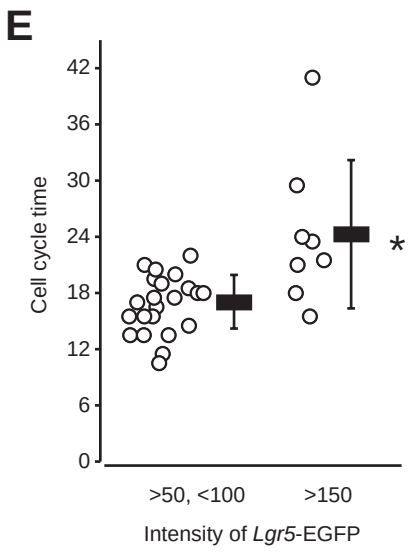
E
Cell cycle time
42
36
30
24
18
12
6
0
*
>50, <100
>150
Intensity of Lgr5-EGFP

Figure S4

Figure S4 Cell cycle times in cells expressed high or low levels of *Lgr5*-EGFP, Related to Figure 3 (A to D) Enteroids were derived from *Lgr5-EGFP-IRES-CreERT2* (+/-) / *Rosa-CAG-LSL-tdTomato-WPRE* (+/-) mice. The enteroids (*Lgr5*-EGFP/tdTomato) express *Lgr5*-EGFP and CreERT2 (Metzger and Chambon, 2001) under the control of an endogenous *Lgr5* promoter. Administration of tamoxifen to the enteroids induced expression of tdTomato under the control of CAG promoter by excision of a stop codon flanked by *loxP* sites located just before the tdTomato gene. *Lgr5*-EGFP/tdTomato enteroids were plated onto glass chamber slide and incubated with 1 μM 4-hydroxytamoxifen (Sigma-Aldrich) for two overnights for the expression of tdTomato before imaging experiments. tdTomato (A), EGFP (B), merged (C), and phase contrast (D) images showing a cell division of tdTomato expressing cell in a *Lgr5*-EGFP/tdTomato enteroid. Scale bar, 100 μm. Arrowheads indicate dividing cells. (E) Cell cycle times in cells expressed high (Intensity (A.U.): >150, n = 8) or low levels (Intensity (A.U.): <150, n = 20) of *Lgr5*-EGFP. * $p < 0.05$, student's t-test. Error bars correspond to the SD.

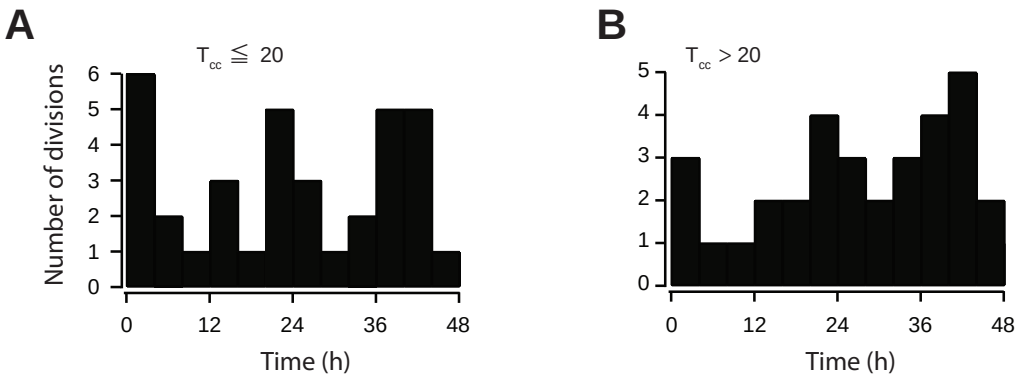
A
$T_{cc} \leqq 20$
Number of divisions
0
1
2
3
4
5
6
0
12
24
36
48
Time (h)
B
$T_{cc} > 20$
0
1
2
3
4
5
0
12
24
36
48
Time (h)

Figure S5

Figure S5 Complex interaction of the circadian clock and the cell cycle, Related to Figure 4
Enteroids from *Lgr5-EGFP-IRES-CreERT2* (+/-) / *Rosa-CAG-LSL-tdTomato-WPRE* (+/-) mice was used. (A) Distribution of the cell divisions whose cell cycle time was shorter than 20 h. (B) Distribution of the cell divisions whose cell cycle time was longer than 20 h.

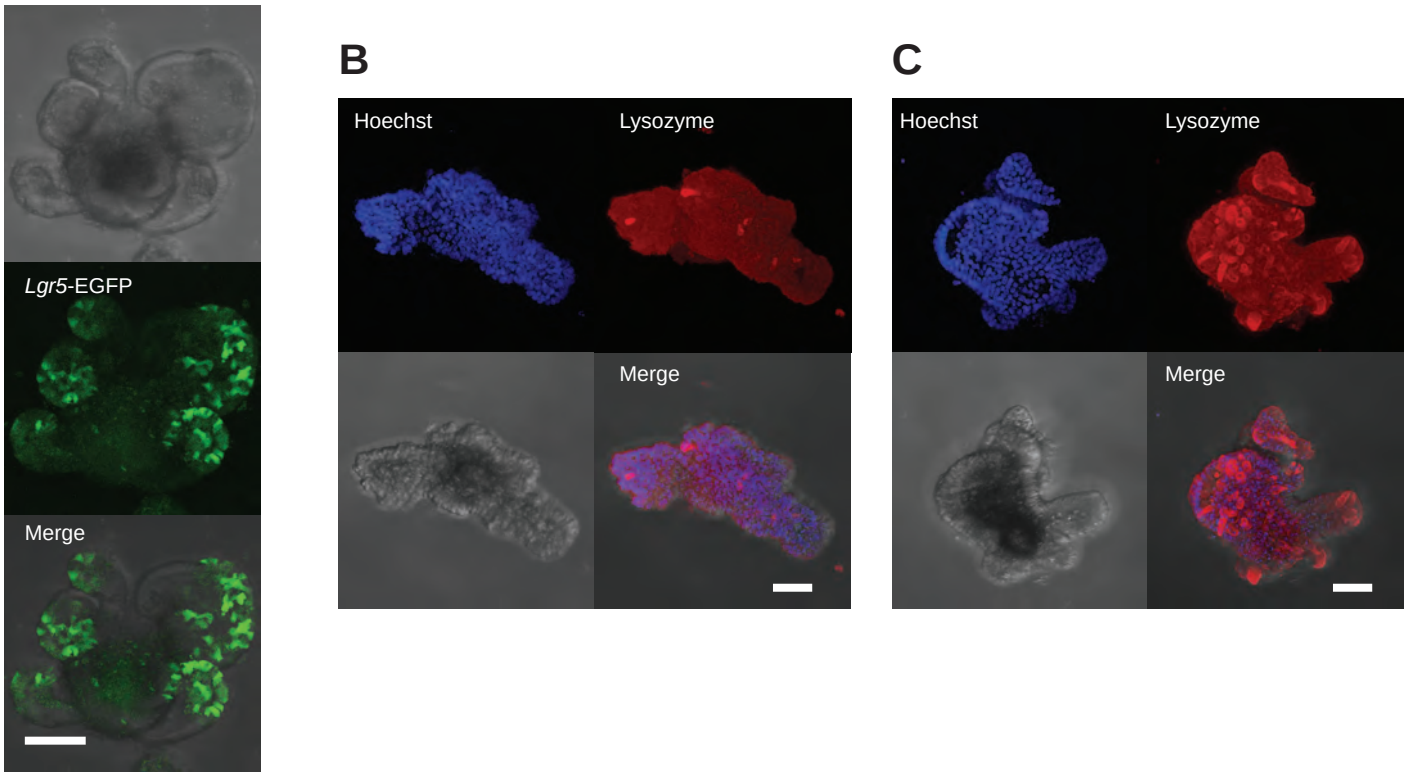
A
Lgr5-EGFP
Merge
B
Hoechst
Lysozyme
Merge
C
Hoechst
Lysozyme
Merge

Figure S6

Figure S6 Stem cell and Paneth cell marker expression in enteroids, Related to Figure 5 (A) Fluorescent images from the enteroid derived from *Lgr5*-EGFP transgenic mice (*Lgr5-EGFP-IRES-CreERT2* (+/-) / *Rosa-CAG-LSL-tdTomato-WPRE* (+/-)) in normal culture condition. Bright field (top panel), EGFP (middle panel), and the merge of bright field and EGFP (bottom panel) images are shown. Scale bar, 50 μm. (B and C) Immunostaining images of PER2::LUC enteroids cultured in stem cell rich (B) or normal (C) condition. Nuclear (Hoechst), Paneth cell (Lysozyme), bright field, and the merge of nuclear, Paneth cell, and bright field images are shown. Scale bar, 50 μm.

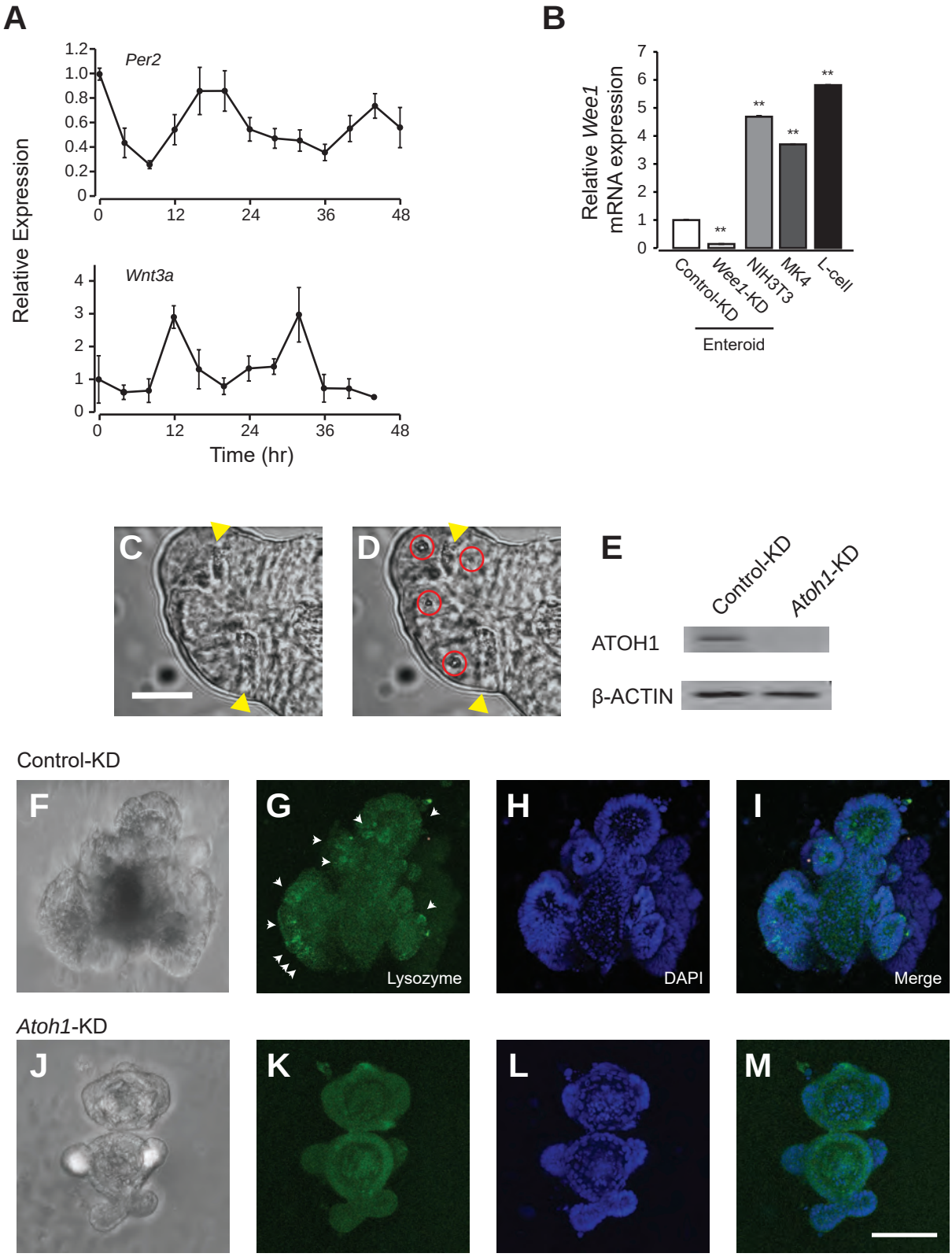
A
Per2
Wnt3a
Relative Expression
Time (hr)
B
Relative Wee1 mRNA expression
Control-KD
Wee1-KD
NIH3T3
MK4
L-cell
Enteroid
C
D
E
Control-KD
Atoh1-KD
ATOH1
β-ACTIN
Control-KD
F
G
Lysozyme
H
DAPI
I
Merge
Atoh1-KD
J
K
L
M

Figure S7

Figure S7 Paneth cell ablation in enteroids, Related to Figure 6 (A) qRT-PCR data of mRNA expressions of *Per2* and *Wnt3a*. n = 3. (B) qRT-PCR results for mRNA expression levels of *Wee1* in control-KD and *Wee1*-KD enteroids, NIH3T3 cells, MK4 cells, and L-cell. The KD efficiency of *Wee1* was 85.8 ± 1.0% (mean ± SD). (C and D) Laser-irradiation of ISCs/PCs. Images of a crypt before (C) and after (D) the laser-irradiation. Arrowheads indicate Paneth cells. Circles indicate pores made by the laser-irradiation. Scale bar, 10 μm. (E) Expression levels of ATOH1 and β-ACTIN in control-KD and *Atoh1*-KD FUCCI2 enteroids were determined by western-blots. The KD efficiency of *Atoh1* was 91.8 ± 13.3% (mean ± SD). (F to M) Immunostaining of Lysozyme, a Paneth cell marker, in control-KD (F to I) and *Atoh1*-KD (J to M) enteroids. DIC (F and J), Lysozyme (G and K), nuclear (DAPI: H and L), and the merge of Lysozyme and nuclear (I and M) images are shown. Scale bar, 100 μm.

Table S1. Primer Sets Used in qRT-PCR, Related to Figure 6.

Gene	**Direction**	**Sequence**
GAPDH	Forward	5'- TGT GTC CGT CGT GGA TCT GA-3'
	Reverse	5'-TTG CTG TTG AAG TCG CAG GAG-3'
Wnt3a	Forward	5'- ACA CTT GAG CAG AAC GGA TAC A-3'
	Reverse	5'-TGG ATA CAG CAG GTT GGT AGG-3'
Per2	Forward	5'-TTC CAC TAT GTG ACA GCG GAG G-3'
	Reverse	5'-CGT ATC CAT TCA TGT CGG GCT C-3'
Cryptdin-1	Forward	5'-TAG TCT CTT CAT CTG TGT TTT GGA TAG G-3'
	Reverse	5'-ACT AGT CCT CCT CTC TGC CCT TGT-3'

Table S2. Antibodies Used in Immunostaining, Related to Figure 6.

Antibodies	**Host**	**Supplier**	**Dilution**	**Catalog no.**
Lysozyme (Figure S7)	Rabbit	Cell Marque	1:100	278A-17
Lysozyme (Figure 6 and S6)	Rabbit	Dako	1:1000	A0099
EGFP	Chicken	Abcam	1:1000	Ab13970
Alexa fluor 488 goat anti-rabbit IgG (Figure S7)	Goat	Life technologies	1:400	A11034
Alexa fluor 594 goat anti-rabbit IgG (Figure 6)	Goat	Life technologies	1:400	A11037
Alexa fluor 488 goat anti-chiken IgG	Goat	Life technologies	1:400	A11039

Supplemental Experimental Procedure

Materials

shRNA expressing lentivirus (MISSION shRNA, Sigma-Aldrich) for mouse *Bmal1* (TRCN0000095055) was obtained from Lenti-shRNA Library Core in Cincinnati Children's hospital Medical Center (CCHMC). Lentiviruses to express Green-Luciferase-hGeminin, *Per2*-Red-Luciferase, mVenus-hGeminin, and *Per2*-mCherry were obtained from Viral Vector Core in CCHMC. PER2::LUC mice on a C57Bl/6J background were obtained from Jackson Laboratories (Bar Harbor, ME, USA) (Yoo et al., 2004). 7TFP plasmid is a gift from Dr. Roel Nusse (Stanford University, Addgene plasmid # 24308). TopFlash stable HEK293 cell line is a gift from Dr. Jeffrey Whitsett (CCHMC).

Animals

Experiments used C57BL/6J (Jackson Laboratory), *Gt(ROSA)26Sortm4*(*ACTB-tdTomato,-EGFP*)*Luo/J* (Jackson Laboratory), *R26-H2B-EGFP* (Riken Acc. No. CDB0238K) (Abe et al., 2011) or *R26p- FUCCI2* (Riken Acc. No. CDB0203T) (Abe et al., 2013), *Lgr5-EGFP-IRES-CreERT2* (+/-) / *Rosa-CAG-LSL-tdTomato-WPRE* (+/-) mice. All mice were housed in the animal facility at Cincinnati Children's Hospital Medical Center (CCHMC). All animal experiments were approved by CCHMC Institutional Animal Care and Use Committee (protocol no. 2013-0173) and performed in accordance with approved ethical guidelines and regulations.

Preparation of enteroids

Using the methods of Sato and colleagues (Sato et al., 2009), we prepared intestinal organoids (enteroids) by isolating fresh mid-jejunal crypts from mice. We sacrificed animals using CO_2 inhalation followed by cervical dislocation. Approximately 6 cm of jejunum was dissected from the mouse, flushed with ice cold PBS and splayed open with scissors. The jejunal segment was then sliced into 1-cm pieces and transferred to 5 ml of cold PBS on ice. This suspension was placed on a rocking table at 4°C for 5 min to remove residual blood or stool from jejunal segments. After rocking, the PBS was aspirated and 5 ml of 2 mM EDTA chelation buffer was added. The suspension was placed back on a rocking table at 4°C for 30 min. Chelation buffer was then removed and 5 ml of shaking buffer (PBS with 43.3 mM sucrose and 54.9 mM sorbitol) was added. The conical tube was gently shaken by hand for 1 min. The intestinal crypt suspension was filtered through a 70-μm cell strainer into a 50 ml conical tube. Intestinal crypts were centrifuged down at 400 G for 5 min and resuspended in Matrigel™ (BD Biosciences, San Jose, CA, USA) plus the growth factors R-spondin (conditioned media) (Mahe et al., 2013), mouse Noggin and mouse EGF (R&D Systems, Minneapolis, MN, USA) and then plated onto tissue culture plates. The Matrigel™ suspension was allowed to polymerize at 37°C for between 15 min and 1 h before fresh minigut medium was supplied. Minigut medium plus growth factors was replaced every 3-4 days. Enteroids were maintained in culture for ~6-9 days before being propagated into additional wells or used for experimental procedures.

Gene constructions

Green-Luciferase-PEST-hGeminin, *Per2*-Red-Luciferase-PEST-PGK-puro^r, and *Per2*-mCherry were constructed using PCR and yeast recombination in pcDNA3.1 (Invitrogen) and then cloned

into EcoRI-XbaI site of CSII-EF-MCS lentivirus plasmid. Green- and Red-Luciferase were fused to proline (P), glutamic acid (E), serine (S), and threonine (T) rich sequence (PEST) to shorten their intracellular half-life.

Lentivirus induction

Enteroids were cultured with minigut medium supplemented with (R&D Systems) for a week before lentivirus induction. Enteroids were treated by accutase (Life technologies) and gently passed through syringe needle (27G). Dissociated cells were suspended in minigut medium supplemented with WNT, 10 μM Y-27632 (ROCK inhibitor, Sigma-Aldrich, St Louis, MO, USA), and lentivirus. *Per2*-RedLuciferase expressing enteroids and *Bmal1*-KD enteroids were selected by puromycin (2 μM).

Bioluminescence recording

Enteroids or fibroblasts were plated on 35 mm plastic dish and placed in a Kronos Dio™ AB-2550 incubating luminometer (ATTO Corporation, Tokyo, Japan) with minigut medium or Dulbecco's modified Eagle's medium and 200 μM Beetle Luciferin K+ salt (Promega, Fitchburg, WI, USA) for real-time periodic quantification of PER2 protein, Green-Luciferase-hGeminin, or *Per2*-Red-Luciferase abundance by bioluminescence recording (Malloy et al., 2012).

WNT secretion from enteroids was measured by TOPFlash promoter luciferase assay (Molenaar et al., 1996) with a reporter plasmid containing TCF/LEF sites upstream of a luciferase (7TFP) (Fuerer and Nusse, 2010). WT enteroids and *Bmal1*-KD enteroids derived from B6 mice were plated into 12-well plates at the start of the experiment. Organoids for each time point were plated into a separate plate to limit manipulation or exposure to possible resetting cues. End of serum shock is indicated by circadian time 0 to compare with bioluminescent recordings performed in parallel. Culturing media was harvested every 4 h over a 48-h period and used for the reporter assay. HEK293 cells were suspended in DMEM containing 10% FBS, 7TFP plasmid and PEI solution for transfection (Reed et al., 2006). The transfected cells were plated into 24-well plates and incubated overnight. Culturing media was changed to 150 μl each of the media harvested from enteroids. 150 μl of fresh DMEM with 10% FBS was further added to each well, and the cells were cultured for two days in CO_2 incubator at 37 °C. 12.5 μM of luciferin was added to each well, and the cells were suspended in media. Luciferase activity was measured with TD20e luminometer (Turner) and normalized by number of cells. WNT secretion from enteroids was also measured by co-culture of WT and *Per1/2*-DKO enteroids and TOPFlash stable HEK293 cells.

Western blot analysis

Enteroids were collected and centrifuged, then matrigel was removed by pipetting. Protein lysate was prepared by lysis of enteroids with RIPA buffer. 20 μg of protein was separated on a 10% polyacrylamide gel and transferred to a PVDF membrane (Immobilon-P, Millipore). Membranes were incubated for 1 h with Odyssey blocking buffer (Li-Cor Biosciences), incubated 1 h at room temperature with anti-β-ACTIN (1:1000 dilution, Cell Signaling), anti-BMAL1 (1:1000 dilution, Bethyl laboratories, Inc.), or anti-ATOH1 (MATH1: 1:1000 dilution, DSHB) antibodies, and then incubated for 1 h in goat anti-mouse or anti-rabbit secondary antibodies

(IRDye 800 or IRDye700, 1:5000 dilution, Li-Cor Biosciences). Blots were quantified using an Odyssey infrared imaging system (Li-Cor Biosciences).

Immunocytochemistry
Control-KD and *Atoh1*-KD enteroids were fixed by ice-cold methanol for 5 min, incubated with rabbit anti-Lysozyme antibody (SIGMA-ALDRICH, 278A-17), and stained by Alexa Fluor 488 conjugate goat anti-rabbit antibody (Life technologies) and DAPI.

Fluorescent imaging
Enteroids were plated on 8-well chamber slide (Lab-tech) two days before imaging experiments. Image acquisition was performed through LSM710 LIVE Duo Confocal Microscope (Zeiss) with a 20x, 0.85 NA, dry objective. For the fluorescent image of FUCCI2 enteroids, sequential excitation of mVenus and mCherry was performed by using a 514-nm and 560-nm lasers, respectively. For the fluorescent image of *Lgr5-EGFP-IRES-CreERT2* (+/-) / *Rosa-CAG-LSL-tdTomato-WPRE* (+/-) enteroids or *Per2*-mCherry expressing H2B-EGFP enteroids, sequential excitation of EGFP and mCherry was performed by using a 488-nm and 560-nm lasers, respectively. Enteroid structure was imaged by reflection of 840-nm laser. For the fluorescent image of immunostained enteroids, sequential excitation of Alexa Fluor 488 and DAPI was performed by using a 488-nm and 400-nm lasers, respectively. Enteroid structure was imaged by reflection of 840-nm laser. For induced expression of tdTomato, *Lgr5*-EGFP/tdTomato enteroids were plated onto glass chamber slide and incubated with 1 μM 4-hydroxytamoxifen (Sigma-Aldrich) for two overnights for the expression of tdTomato before imaging experiments. Single cell ablations of enteroid cells were performed through LSM510 tow-photon microscope (Zeiss) with a 40x, 1.40 NA, water immersion objective. For the laser-irradiation of single cells, repeated scans (200 times) of defined regions were performed by using a 730-nm laser with maximum laser output power.

qPCR
PER2::LUC enteroids and *Bmal1*-KD B6 enteroids were plated into 12-well plates at the start of the experiment. Organoids for each time point were plated into a separate plate to limit manipulation or exposure to possible resetting cues. End of serum shock is indicated by circadian time 0 to compare with bioluminescent recordings performed in parallel. RNA was harvested every 4 h over a 48-h period using 0.25 ml/well of TRI Reagent™ RT (Molecular Research Center, Cincinnati, OH, USA). Total RNA was treated with RQ1 DNaseI (Promega, Fitchburg, WI, USA). For reverse transcription reactions, 1 μg of total RNA was used with GoScript Reverse Transcriptase (Promega) according to manufacturer's instructions. qPCR was performed with SYBR Green Master Mix (Qiagen, Germantown, MD, USA) using primers listed in Table S1. qPCR results were detected by using the StepOnePlus System (Life Technologies, Grand Island, NY, USA).

Data analysis
Counting the number of fluorescent protein expressing cells, single cell tracking, and fluorescent intensity detection in single cells were performed by Imaris software (Bitplane). Real-time luminescent signal was detrended by Kronos software (ATTO).

Fast Fourier transform (FFT) analysis

Fast Fourier transform (FFT) analysis (Cooley, 1965) for the time course changes of the number of mVenus-hGeminin positive cells or luciferase signal was performed using R statistical software. To perform Fast Fourier Transformation, the data is assumed to be continuous repeats of sequence data. One could expect a minor peak at 24-hour for FFT analysis from the analysis of our Green-Luc-hGeminin cell cycle data, but the appearance of these small peaks depends on noise and baseline movements, which produces other minor peaks. We observe that four out of eight experimental data exhibit a minor peak at around 24 hours (Figure S1).

Coupled mathematical model of circadian clock and cell cycle

For our simulations, we adopted the coupled model of circadian clock and cell cycle (Zamborszky et al., 2007). The equations for the circadian clock module of the coupled model are:

$$\frac{\mathrm{d}[\mathrm{M}]}{\mathrm{d}t} = k_{ms}\frac{[\mathrm{TF}]^{\mathrm{n}}}{J^{\mathrm{n}} + [\mathrm{TF}]^{\mathrm{n}}} - k_{md}[\mathrm{M}]$$

$$\frac{\mathrm{d}[\mathrm{CP}]}{\mathrm{d}t} = k_{cps}[\mathrm{M}] - k_{cpd}[\mathrm{CP}] - 2k_a[\mathrm{CP}]^2 + 2k_d[\mathrm{CP}_2] - k_{p1}\frac{[\mathrm{CP}]}{J_p + [\mathrm{CP}_T]}$$

$$\frac{\mathrm{d}[\mathrm{CP}_2]}{\mathrm{d}t} = k_a[\mathrm{CP}]^2 - k_d[\mathrm{CP}_2] - k_{cp2d}[\mathrm{CP}_2] + k_{icd}[\mathrm{IC}] - k_{ica}[\mathrm{CP}_2][\mathrm{TF}] - k_{p2}\frac{[\mathrm{CP}_2]}{J_p + [\mathrm{CP}_T]}$$

$$\frac{\mathrm{d}[\mathrm{TF}]}{\mathrm{d}t} = k_{cp2d}[\mathrm{IC}] + k_{icd}[\mathrm{IC}] - k_{ica}[\mathrm{CP}_2][\mathrm{TF}] + k_{p2}\frac{[\mathrm{IC}]}{J_p + [\mathrm{CP}_T]}$$

Definitions:

$$[\mathrm{IC}] = [\mathrm{TF}_T] - [\mathrm{TF}]$$

$$[\mathrm{CP}_T] = [\mathrm{CP}] + 2[\mathrm{CP}_2] + 2[\mathrm{IC}]$$

Rate constants (h^{-1}):

k_{ms} = 1, k_{md} = 0.1, k_{cps} =0.5, k_{cpd} = 0.525, k_a = 100, k_d = 0.01, k_{cp2d} =0.0525, k_{icd} = 0.01, k_{ica} = 20, k_{p1} = 10, k_{p2} = 0.1

Dimensionless constants:

$[\mathrm{TF}_T]$ = 0.5, J_p = 0.05, J = 0.3, n = 2

The equations for the cell cycle module of the coupled model are:

$$\frac{\mathrm{d}[\mathrm{CycD}]}{\mathrm{d}t} = \varepsilon\left(k'_{w4} + k_{w4}[\mathrm{M}]\right) + V_6[\mathrm{CycD:p21}] + k_{24r}[\mathrm{CycD:p21}] - k_{24}[\mathrm{CycD}][\mathrm{p21}] - k_{10}[\mathrm{CycD}]$$

$$\frac{\mathrm{d}[\mathrm{CycD:p21}]}{\mathrm{d}t} = k_{24}[\mathrm{CycD}][\mathrm{p21}] - k_{24r}[\mathrm{CycD:p21}] - V_6[\mathrm{CycD:p21}] - k_{10}[\mathrm{CycD:p21}]$$

$$\frac{\mathrm{d}[\mathrm{CycE}]}{\mathrm{d}t} = \varepsilon\left(k'_7 + k_7[\mathrm{E2F}_A]\right)[\mathrm{mass}] - V_8[\mathrm{CycE}] - k_{25}[\mathrm{CycE}][\mathrm{p21}] + k_{25r}[\mathrm{CycE:p21}] + V_6[\mathrm{CycE:p21}]$$

$$\frac{\mathrm{d}[\mathrm{CycE:p21}]}{\mathrm{d}t} = k_{25}[\mathrm{CycE}][\mathrm{p21}] - k_{25r}[\mathrm{CycE:p21}] - V_6[\mathrm{CycE:p21}] - V_8[\mathrm{CycE:p21}]$$

$$\frac{\mathrm{d}[\mathrm{CycA}]}{\mathrm{d}t} = \varepsilon k_{29}[\mathrm{E2F}_A] - k_{30}[\mathrm{Cdc20}][\mathrm{CycA}] - k_{25}[\mathrm{CycA}][\mathrm{p21}] + k_{25r}[\mathrm{CycA:p21}] + V_6[\mathrm{CycA:p21}]$$

$$\frac{\mathrm{d}[\mathrm{CycA:p21}]}{\mathrm{d}t} = k_{25}[\mathrm{CycA}][\mathrm{p21}] - k_{25r}[\mathrm{CycA:p21}] - V_6[\mathrm{CycA:p21}] - \mathrm{k}_{30}[\mathrm{Cdc20}][\mathrm{CycA:p21}]$$

$$\frac{\mathrm{d}[\mathrm{p21}]}{\mathrm{d}t} = \varepsilon\left(k'_{w3} + k_{w3}\frac{K_{p21}^2}{K_{p21}^2 + [\mathrm{M}]^2}\right) - V_6[\mathrm{p21}] - k_{24}[\mathrm{CycD}][\mathrm{p21}] + k_{24r}[\mathrm{CycD:p21}] + k_{10}[\mathrm{CycD:p21}]$$
$$- k_{25}[\mathrm{p21}]\left([\mathrm{CycE}] + [\mathrm{CycA}]\right) + k_{25r}\left([\mathrm{CycE:p21}] + [\mathrm{CycA:p21}]\right) + V_8[\mathrm{CycE:p21}] + k_{30}[\mathrm{Cdc20}][\mathrm{CycA:p21}]$$

$$\frac{\mathrm{d}[\mathrm{E2F}]}{\mathrm{d}t} = k_{22}\left([\mathrm{E2F}_T] - [\mathrm{E2F}]\right) - \left(k'_{23} + k_{23}\left([\mathrm{CycA}] + [\mathrm{CycB}]\right)\right)[\mathrm{E2F}]$$

$$\frac{\mathrm{d}[\mathrm{CycB}]}{\mathrm{d}t} = \varepsilon\left(k'_1 + \frac{k_1\left([\mathrm{CycB}]/J_1\right)^2}{1 + \left([\mathrm{CycB}]/J_1\right)^2}\right)[\mathrm{mass}] - V_2[\mathrm{CycB}] + \left(k'_{cdc25} + k_{cdc25}[\mathrm{Cdc25a}]\right)[\mathrm{CycBP}]$$
$$- \left(k'_{wee1} + k_{wee1}[\mathrm{Wee1}]\right)[\mathrm{CycB}]$$

$$\frac{\mathrm{d}[\mathrm{CycBP}]}{\mathrm{d}t} = \left(k'_{wee1} + k_{wee1}[\mathrm{Wee1}]\right)[\mathrm{CycB}] - \left(k'_{cdc25} + k_{cdc25}[\mathrm{Cdc25a}]\right)[\mathrm{CycBP}] - V_2[\mathrm{CycBP}]$$

$$\frac{\mathrm{d}[\mathrm{Wee1}]}{\mathrm{d}t} = \left(k'_{w5} + k_{w5}[\mathrm{M}]\right) - \left(k'_{w2} + k_{w2}[\mathrm{CycB}]\right)\frac{[\mathrm{Wee1}]}{J_{w2} + [\mathrm{Wee1}]} + k_{w1}\frac{[\mathrm{Wee1P}]}{\mathrm{J}_{\mathrm{w1}} + [\mathrm{Wee1P}]} - k_{w6}[\mathrm{Wee1}]$$

$$\frac{\mathrm{d}[\mathrm{Wee1P}]}{\mathrm{d}t} = \left(k'_{w2} + k_{w2}[\mathrm{CycB}]\right)\frac{[\mathrm{Wee1}]}{J_{w2} + [\mathrm{Wee1}]} - k_{w1}\frac{[\mathrm{Wee1P}]}{J_{w1} + [\mathrm{Wee1P}]} - k_{wd}[\mathrm{Wee1P}]$$

$$\frac{\mathrm{d}[\mathrm{Cdc25a}]}{\mathrm{d}t} = \left(k'_{c3} + k_{c3}[\mathrm{CycB}]\right)\frac{1 - [\mathrm{Cdc25a}]}{J_{c3} + 1 - [\mathrm{Cdc25a}]} - k_{c4}\frac{[\mathrm{Cdc25a}]}{J_{c4} + [\mathrm{Cdc25a}]}$$

$$\frac{\mathrm{d}[\mathrm{Cdh1}]}{\mathrm{d}t} = \left(k'_3 + k_3[\mathrm{Cdh20}]\right)\frac{1 - [\mathrm{Cdh1}]}{J_3 + 1 - [\mathrm{Cdh1}]} - V_4\frac{[\mathrm{Cdh1}]}{J_4 + [\mathrm{Cdh1}]}$$

$$\frac{\mathrm{d}[\mathrm{Cdc20_T}]}{\mathrm{d}t} = \varepsilon\left(k'_{11} + k_{11}[\mathrm{CycB}]\right) - k_{12}[\mathrm{Cdc20}_T]$$

$$\frac{\mathrm{d}[\mathrm{Cdc20}]}{\mathrm{d}t} = k_{13}[\mathrm{IEP}]\frac{[\mathrm{Cdc20}_T]-[\mathrm{Cdc20}]}{J_{13}+[\mathrm{Cdc20}_T]-[\mathrm{Cdc20}]} - k_{14}\frac{[\mathrm{Cdc20}]}{J_4+[\mathrm{Cdc20}]} - k_{12}[\mathrm{Cdc20}]$$

$$\frac{\mathrm{d}[\mathrm{PPX}]}{\mathrm{d}t} = \varepsilon k_{33} - k_{34}[\mathrm{PPX}]$$

$$\frac{\mathrm{d}[\mathrm{IEP}]}{\mathrm{d}t} = k_{31}[\mathrm{CycB}]\frac{1-[\mathrm{IEP}]}{J_{31}+1-[\mathrm{IEP}]} - k_{32}[\mathrm{PPX}]\frac{[\mathrm{IEP}]}{J_{32}+[\mathrm{IEP}]}$$

$$\frac{\mathrm{d}[\mathrm{GM}]}{\mathrm{d}t} = k_{27}[\mathrm{mass}]\mathrm{H}\left(\frac{[\mathrm{Rb}_{hypo}]}{[\mathrm{Rb}_T]}\right) - k_{28}[\mathrm{GM}]$$

$$\frac{\mathrm{d}[\mathrm{mass}]}{\mathrm{d}t} = \varepsilon\mu[\mathrm{GM}]$$

To simulate P21 regulation of G2/M transition, we assumed inhibitory binding of P21 with CycB/Cdk1 (Bates et al., 1998; Medema et al., 1998; Niculescu et al., 1998). We included the equation for the CycB:P21 complex into the cell cycle module and updated the equations for CycB and P21 as follows:

$$\frac{\mathrm{d}[\mathrm{p21}]}{\mathrm{d}t} = \varepsilon\left(k'_{w3} + k_{w3}\frac{K_{p21}^2}{K_{p21}^2+[\mathrm{M}]^2}\right) - V_6[\mathrm{p21}] - k_{24}[\mathrm{CycD}][\mathrm{p21}] + k_{24r}[\mathrm{CycD:p21}] + k_{10}[\mathrm{CycD:p21}]$$
$$- k_{25}[\mathrm{p21}]([\mathrm{CycE}]+[\mathrm{CycA}]+[\mathrm{CycB}]) + k_{25r}([\mathrm{CycE:p21}]+[\mathrm{CycA:p21}]+[\mathrm{CycB:p21}]) + V_2[\mathrm{CycB:p21}]$$
$$+ V_8[\mathrm{CycE:p21}] + k_{30}[\mathrm{Cdc20}][\mathrm{CycA:p21}]$$

$$\frac{\mathrm{d}[\mathrm{CycB}]}{\mathrm{d}t} = \varepsilon\left(k'_1 + \frac{k_1([\mathrm{CycB}]/J_1)^2}{1+([\mathrm{CycB}]/J_1)^2}\right)[\mathrm{mass}] - V_2[\mathrm{CycB}] - k_{25}[\mathrm{CycB}][\mathrm{p21}] + k_{25r}[\mathrm{CycB:p21}]$$
$$+ V_6[\mathrm{CycB:p21}] + (k'_{\mathrm{cdc25}} + k_{\mathrm{cdc25}}[\mathrm{Cdc25a}])[\mathrm{CycBP}] - (k'_{wee1} + k_{wee1}[\mathrm{Wee1}])[\mathrm{CycB}]$$

$$\frac{\mathrm{d}[\mathrm{CycB:p21}]}{\mathrm{d}t} = k_{25}[\mathrm{CycB}][\mathrm{p21}] - k_{25r}[\mathrm{CycB:p21}] - V_6[\mathrm{CycB:p21}] - V_2[\mathrm{CycB:p21}]$$

Recent work by Yao et al (Yao et al., 2008) revealed that the CycD level is gradually elevated when the level of the growth factors increases, and this regulation is incorporated in the current model. One of the growth factors (WNT) is under the control by the circadian clock and couples the cell cycle with the circadian clock.

How cell size is controlled is not completely understood (Ginzberg et al., 2015). In the current model, we have made a simplifying assumption that the cell size controls the entry into the cell cycle as well as cell division. In this way, the cell growth and the cell cycle are coupled, and the cells neither grow to a very large size without division nor divide to too small a size to survive.

Steady-state relations:

$$[\mathrm{PP1}_A] = \frac{[\mathrm{PP1}_T]}{1 + K_{21}\left(\varphi_E\left([\mathrm{CycE}] + [\mathrm{CycA}]\right) + \varphi_B[\mathrm{CycB}]\right)}$$

$$[\mathrm{Rb}_{hypo}] = \frac{[\mathrm{Rb}_T]}{1 + \dfrac{k_{20}\left(\lambda_D[\mathrm{CycD}_T] + \lambda_E[\mathrm{CycE}] + \lambda_A[\mathrm{CycA}] + \lambda_B[\mathrm{CycB}]\right)}{k'_{19}\left([\mathrm{PP1}_T] - [\mathrm{PP1}_A]\right) + k_{19}[\mathrm{PP1}_A]}}$$

$$[\mathrm{E2F}_A] = \frac{\left([\mathrm{E2F}_T] - [\mathrm{E2F:Rb}]\right)[\mathrm{E2F}]}{[\mathrm{E2F}_T]}$$

$$[\mathrm{E2F:Rb}] = \frac{2[\mathrm{E2F}_T][\mathrm{Rb}_{hypo}]}{[\mathrm{E2F}_T] + [\mathrm{Rb}_{hypo}] + L + \sqrt{\left([\mathrm{E2F}_T] + [\mathrm{Rb}_{hypo}] + L\right)^2 - 4[\mathrm{E2F}_T][\mathrm{Rb}_{hypo}]}}$$

Definitions:

$$V_2 = k'_2\left(1 - [\mathrm{Cdh1}]\right) + k_2[\mathrm{Cdh1}] + k''_2[\mathrm{Cdc20}]$$

$$V_4 = k_4\left(\gamma_A[\mathrm{CycA}] + \gamma_B[\mathrm{CycB}]\right)$$

$$V_6 = k'_6 + k_6\left(\eta_E[\mathrm{CycE}] + \eta_A[\mathrm{CycA}] + \eta_B[\mathrm{CycB}]\right)$$

$$V_8 = k'_8 + \frac{k_8\left(\psi_E\left([\mathrm{CycE}] + [\mathrm{CycA}]\right) + \psi_B[\mathrm{CycB}]\right)}{J_8 + [\mathrm{CycE}_T]}$$

$$L = \frac{k_{26r}}{k_{26}} + \frac{k_{20}}{k_{26}}\left(\lambda_D[\mathrm{CycD}_T] + \lambda_E[\mathrm{CycE}] + \lambda_A[\mathrm{CycA}] + \lambda_B[\mathrm{CycB}]\right)$$

Rate constants (h^{-1}):

$k_1' = 0.1$, $k_1 = 0.6$, $k_2' = 0.05$, $k_2 = 20$, $k_2'' = 1$, $k_3' = 7.5$, $k_3 = 140$, $k_4 = 40$, $k_5 = 20$, $k_6' = 10$, $k_6 = 100$, $k_7' = 0$, $k_7 = 0.6$, $k_8' = 0.1$, $k_8 = 2$, $k_9 = 2.5$, $k_{10} = 5$, $k_{11}' = 0$, $k_{11} = 1.5$, $k_{12} = 1.5$, $k_{13} = 5$, $k_{14} = 2.5$, $k_{15} = 0.25$, $k_{16} = 0.25$, $k_{17}' = 0.35$, $k_{17} = 10$, $k_{18} = 10$, $k_{19}' = 0$, $k_{19} = 20$, $k_{20} = 10$, $k_{22} = 1$, $k_{23}' = 0.005$, $k_{23} = 1$, $k_{24} = 1000$, $k_{24r} = 10$, $k_{25} = 1000$, $k_{25r} = 10$, $k_{26} = 10000$, $k_{26r} = 200$, $k_{27} = 0.2$, $k_{28} = 0.2$, $k_{29} = 0.05$, $k_{30} = 20$, $k_{31} = 0.7$, $k_{32} = 1.8$, $k_{33} = 0.05$, $k_{34} = 0.05$, $\mu = 0.061$, $k_{cdc25}' = 0.05$, $k_{cdc25} = 10$, $k_{c3}' = 0.1$, $k_{c3} = 1$, $k_{c4} = 0.4$, $k_{w1} = 0.4$, $k_{wee1}' = 0.08$, $k_{wee1} = 10$, $k_{w2}' = 0.2$, $k_{w2} = 2$, $k_{w6} = 1$, $k_{wd} = 1$.

Dimensionless constants:

$J_1 = 0.1$, $J_3 = J_4 = 0.01$, $J_8 = 0.1$, $J_{13} = J_{14} = 0.005$, $J_{15} = 0.1$, $J_{17} = 0.3$, $J_{31} = J_{32} = 0.01$, $J_{c3} = J_{c4} = 0.05$, $J_{w1} = J_{w2} = 0.2$, $K_{21} = 1$, $[\mathrm{E2F}_T] = 5$, $[\mathrm{PP1}_T] = 1$, $[\mathrm{Rb}_T] = 10$, $\varphi_E = 25$, $\varphi_B = 2$, $\gamma_A = 0.3$, $\gamma_B = 1$, $\eta_E = 0.5$, $\eta_A = 0.5$, $\eta_B = 1$, $\lambda_D = 3.3$, $\lambda_E = 5$, $\lambda_A = 3$, $\lambda_B = 5$, $\psi_E = 1$, $\psi_B = 0.05$, $\varepsilon = 1$.

WNT coupling parameters:

1. Zero coupling: $k_{w4}' = 2$, $k_{w4} = 0$

2. Weak coupling: $k_{w4}' = 2$, $k_{w4} = 0.25$
3. Intermediate coupling: $k_{w4}' = 1$, $k_{w4} = 1$
4. Strong coupling: $k_{w4}' = 0$, $k_{w4} = 2$
5. Very strong coupling: $k_{w4}' = 0$, $k_{w4} = 3$

WEE1 coupling parameters:

1. Zero coupling: $k_{w5}' = 1$, $k_{w5} = 0$
2. Weak coupling: $k_{w5}' = 1$, $k_{w5} = 0.25$
3. Intermediate coupling: $k_{w5}' = 0.5$, $k_{w5} = 1$
4. Strong coupling: $k_{w5}' = 0.25$, $k_{w5} = 2$
5. Very strong coupling: $k_{w5}' = 0.25$, $k_{w5} = 3$

P21 coupling parameters:

1. Zero coupling: $k_{w3}' = 20$, $k_{w3} = 0$
2. Weak coupling: $k_{w3}' = 15$, $k_{w3} = 5$
3. Intermediate coupling: $k_{w3}' = 10$, $k_{w3} = 20$
4. Strong coupling: $k_{w3}' = 0$, $k_{w3} = 60$
5. Very strong coupling: $k_{w3}' = 0$, $k_{w3} = 80$

For the simulations in the coupled clock and cell cycle model we further assumed that 65% of the cells are strongly coupled to the clock and the remaining 35% of the cells are weakly coupled to the clock. Computer simulations were performed in XPPAUT (Ermentrout, 2002) using Euler method and time step of 0.0005 h. Data analysis was performed in MATLAB (MathWorks, Natick, MA).

Supplementary References

Abe, T., Kiyonari, H., Shioi, G., Inoue, K., Nakao, K., Aizawa, S., and Fujimori, T. (2011). Establishment of conditional reporter mouse lines at ROSA26 locus for live cell imaging. Genesis *49*, 579-590.

Abe, T., Sakaue-Sawano, A., Kiyonari, H., Shioi, G., Inoue, K., Horiuchi, T., Nakao, K., Miyawaki, A., Aizawa, S., and Fujimori, T. (2013). Visualization of cell cycle in mouse embryos with Fucci2 reporter directed by Rosa26 promoter. Development *140*, 237-246.

Bates, S., Ryan, K.M., Phillips, A.C., and Vousden, K.H. (1998). Cell cycle arrest and DNA endoreduplication following p21Waf1/Cip1 expression. Oncogene *17*, 1691-1703.

Cooley, J.W., Tukey, J.W (1965). An algorithm for the machine calculation of complex Fourier series. Mathematics of Computation *19*, 297-301.

Ermentrout, G.B. (2002). Simulating, Analyzing, and Animating Dynamical Systems: A Guide to XPPAUT for Researchers and Students (siam).

Fuerer, C., and Nusse, R. (2010). Lentiviral vectors to probe and manipulate the Wnt signaling pathway. PLoS One *5*, e9370.

Ginzberg, M.B., Kafri, R., and Kirschner, M. (2015). Cell biology. On being the right (cell) size. Science *348*, 1245075.

Grechez-Cassiau, A., Rayet, B., Guillaumond, F., Teboul, M., and Delaunay, F. (2008). The circadian clock component BMAL1 is a critical regulator of p21WAF1/CIP1 expression and hepatocyte proliferation. J. Biol. Chem. *283*, 4535-4542.

Mahe, M.M., Aihara, E., Schumacher, M.A., Zavros, Y., Montrose, M.H., Helmrath, M.A., Sato, T., and Shroyer, N.F. (2013). Establishment of Gastrointestinal Epithelial Organoids. Curr. Protoc. Mouse Biol. *3*, 217-240.

Malloy, J.N., Paulose, J.K., Li, Y., and Cassone, V.M. (2012). Circadian rhythms of gastrointestinal function are regulated by both central and peripheral oscillators. Am. J. Physiol. Gastrointest. Liver Physiol. *303*, G461-473.

Medema, R.H., Klompmaker, R., Smits, V.A., and Rijksen, G. (1998). p21waf1 can block cells at two points in the cell cycle, but does not interfere with processive DNA-replication or stress-activated kinases. Oncogene *16*, 431-441.

Metzger, D., and Chambon, P. (2001). Site- and time-specific gene targeting in the mouse. Methods *24*, 71-80.

Molenaar, M., van de Wetering, M., Oosterwegel, M., Peterson-Maduro, J., Godsave, S., Korinek, V., Roose, J., Destree, O., and Clevers, H. (1996). XTcf-3 transcription factor mediates beta-catenin-induced axis formation in Xenopus embryos. Cell *86*, 391-399.

Niculescu, A.B., 3rd, Chen, X., Smeets, M., Hengst, L., Prives, C., and Reed, S.I. (1998). Effects of p21(Cip1/Waf1) at both the G1/S and the G2/M cell cycle transitions: pRb is a critical determinant in blocking DNA replication and in preventing endoreduplication. Mol. Cell Biol. *18*, 629-643.

Reed, S.E., Staley, E.M., Mayginnes, J.P., Pintel, D.J., and Tullis, G.E. (2006). Transfection of mammalian cells using linear polyethylenimine is a simple and effective means of producing recombinant adeno-associated virus vectors. J. Virol. Methods *138*, 85-98.

Sato, T., Vries, R.G., Snippert, H.J., van de Wetering, M., Barker, N., Stange, D.E., van Es, J.H., Abo, A., Kujala, P., Peters, P.J.*, et al.* (2009). Single Lgr5 stem cells build crypt-villus structures in vitro without a mesenchymal niche. Nature *459*, 262-265.

Yao, G., Lee, T.J., Mori, S., Nevins, J.R., and You, L. (2008). A bistable Rb-E2F switch underlies the restriction point. Nat. Cell Biol. *10*, 476-482.
Yoo, S.H., Yamazaki, S., Lowrey, P.L., Shimomura, K., Ko, C.H., Buhr, E.D., Siepka, S.M., Hong, H.K., Oh, W.J., Yoo, O.J.*, et al.* (2004). PERIOD2::LUCIFERASE real-time reporting of circadian dynamics reveals persistent circadian oscillations in mouse peripheral tissues. Proc. Natl. Acad. Sci. USA *101*, 5339-5346.
Zamborszky, J., Hong, C.I., and Csikasz Nagy, A. (2007). Computational analysis of mammalian cell division gated by a circadian clock: quantized cell cycles and cell size control. J. Biol. Rhythms *22*, 542-553.